



HAL
open science

Green synthesis and characterization of $\text{Li}_{0.5-0.5x}\text{Mg}_x\text{Fe}_{2.5-0.5x}\text{O}_4$ ($0.0 \leq x \leq 1.0$) nano ferrite

Priyanka Tiwari, Shashank Kane, Rulan Verma, Frédéric Mazaleyrat

► To cite this version:

Priyanka Tiwari, Shashank Kane, Rulan Verma, Frédéric Mazaleyrat. Green synthesis and characterization of $\text{Li}_{0.5-0.5x}\text{Mg}_x\text{Fe}_{2.5-0.5x}\text{O}_4$ ($0.0 \leq x \leq 1.0$) nano ferrite. *Advances in basic Science (ICABS 2019)*, Feb 2019, Bahal, India. pp.150018, 10.1063/1.5122567 . hal-04452935

HAL Id: hal-04452935

<https://hal.science/hal-04452935>

Submitted on 12 Feb 2024

HAL is a multi-disciplinary open access archive for the deposit and dissemination of scientific research documents, whether they are published or not. The documents may come from teaching and research institutions in France or abroad, or from public or private research centers.

L'archive ouverte pluridisciplinaire **HAL**, est destinée au dépôt et à la diffusion de documents scientifiques de niveau recherche, publiés ou non, émanant des établissements d'enseignement et de recherche français ou étrangers, des laboratoires publics ou privés.

Copyright

RESEARCH ARTICLE | AUGUST 29 2019

Green synthesis and characterization of $\text{Li}_{0.5-0.5x}\text{Mg}_x\text{Fe}_{2.5-0.5x}\text{O}_4$ ($0.0 \leq x \leq 1.0$) nano ferrite

P. Tiwari; S. N. Kane ; R. Verma; F. Mazaleyrat

 Check for updates

AIP Conf. Proc. 2142, 150018 (2019)

<https://doi.org/10.1063/1.5122567>



View
Online



Export
Citation

CrossMark



Cut Hall measurement time in *half*
using an M91 FastHall™ controller



Also available as part of a tabletop system and an option for your PPMS® system

Green Synthesis and Characterization Of $\text{Li}_{0.5-0.5x}\text{Mg}_x\text{Fe}_{2.5-0.5x}\text{O}_4$ ($0.0 \leq x \leq 1.0$) Nano Ferrite

P. Tiwari^{1,2}, S. N. Kane^{1, a)}, R. Verma¹ and F. Mazaleyrat³

¹Magnetic Materials Laboratory, School of Physics, D. A. University, Khandwa road, Indore – 452001, India.

²Department of Physics, Prestige Institute of Engineering Management and Research, Indore - 452010, India.

³SATIE, ENS Cachan, CNRS 8029, Universite Paris-Saclay, 61 Av. du Pdt. Wilson, F-94230, Cachan, France.

^{a)}Corresponding author: kane_sn@yahoo.com

Abstract. We report synthesis of $\text{Li}_{0.5-0.5x}\text{Mg}_x\text{Fe}_{2.5-0.5x}\text{O}_4$ ($x = 0.0, 0.1, 0.4, 0.6, 0.8, 1.0$) ferrite, utilizing honey green synthesis via sol gel auto combustion method (*without any post-preparation thermal treatment*). X-ray diffraction (XRD), vibrating sample magnetometer (VSM) were used to monitor structural, magnetic properties. XRD validates the formation of nanocrystalline spinel phase with Scherrer's grain diameter varies between 21.5 – 27.9 nm. Results reveal that Mg^{2+} addition: i) changes experimental lattice parameter (a_{exp}), showing incorporation of Mg^{2+} ion in the spinel lattice, ii) changes the cation distribution showing presence of that both Li^{1+} , Mg^{2+} ions on A, B site, iii) modifies inversion parameter (δ) shows transition from inverse to mixed spinel structure, leads to reduction of saturation magnetization (M_s (exp)), iv) alters M_s , understood in terms of cationic redistribution at A, B-sites, v) alters coercivity (H_c), range between 101.4 – 889.9 Oe, vi) shows similar trend of both experimental ' M_s (exp)', theoretical ' M_s (θ)' saturation magnetization, reveal that magnetization behavior of the studied samples is governed by Néel model.

INTRODUCTION, EXPERIMENTAL DETAILS, AND DATA ANALYSIS

Ferrite are insulating magnetic oxide and possess high electrical resistivity, low eddy current, dielectric losses, high saturation magnetization and high permeability. Therefore ferrite materials have application in almost every field such as high frequency devices, microwave devices, bioscience (hyperthermia, MRI), switching devices, gas sensing, multi-layer chip inductor etc. [1-4]. Spinel ferrites display face centred cubic (fcc) structure comprise of two sub-lattices A (tetrahedral) and B (octahedral). Occupation of ions on site A, B (*which affects both structural and magnetic properties*) is a complex process and strongly depends on synthesis process, composition, presence of a particular cation, post-preparation treatments etc. It is important to achieve proper information about occupation of various cations on A,B site. In this situation, x-ray diffraction (XRD) has recognized as one of the most suitable and successful tools for proper determination of cation distribution [5,6,7], although the success of XRD is somewhat limited by the comparable scattering factors of some of the cations present in the spinel structure.

Currently, there is a need to investigate simple, cost-effective, eco-friendly techniques to synthesize nanocrystalline spinel ferrites. Literature reports bio-synthetic protocols utilizing microorganisms, plant extracts etc., has come out as rather straightforward and feasible alternative to physical procedures, and chemical synthetic methods. Literature also reports the use of undemanding synthesis procedure utilizing efficient green precursors e. g.- banana peel, honey, garlic, ginger, neem (*Azadirachta indica*) leaves, cardamom seeds, and aloe vera plant extract, given superior yield of nano-ferrites, displaying appropriate magnetic properties [8]. It is of value to note that, the presence of carbohydrates, flavonoids, phenols, polysaccharides, amino acids, terpenoids, etc. in plant extracts acts as chelating agent, stabilizing agent, capping agents, [9], needed for the synthesis of ferrite nano particles via sol gel auto combustion method. In addition toxicity of nano-particles can be reduced via green synthesis, making them attractive for bio-medical applications, due to better biocompatibility [10].

Li-ferrite has inverse spinel structure with Li-ion have a preference to occupy octahedral B-site and Fe ions occupy both A, B-site. Li-ferrites are used in many electronic devices such as inductors, converters or

electromagnetic wave absorbers, phase-shifters, radar, etc. in the radio frequency range due to their high Curie temperature, high saturation magnetization and squareness in their hysteresis loop. Literature reports study of Li-Co [11], Li-Mg [12], Li-Cd [13,14], Li-Zn [15] ferrites, where properties of Li ferrites was modified by doping various ions. Substitution of ions increases squareness of hysteresis loop of Li-ferrite leads to increase of coercivity (H_c). It is worth noting that, due to lower melting point of Li ($\sim 180^\circ\text{C}$), in order to preserve the stoichiometry, there is a need for either lower temperature sintering or no sintering. To meet this requirement during synthesis, sol gel auto combustion technique is of use to facilitate the formation of the spinel phase, and also has the advantage of energy efficient synthesis. Although literature reports Li-based ferrites, however green synthesis utilizing sol-gel auto-combustion method (where no post-preparation synthesis was used) is less-explored in the literature. Thus in this work, we report synthesis of $\text{Li}_{0.5-0.5x}\text{Mg}_x\text{Fe}_{2.5-0.5x}\text{O}_4$ ($x = 0.0, 0.1, 0.4, 0.6, 0.8, 1.0$) ferrite, utilizing honey green synthesis via sol gel auto combustion method (*without any post-preparation thermal treatment*), and their structural (*via x-ray diffraction*), magnetic characterization (*via vibrating sample magnetometer 'VSM'*).

Sol gel auto-combustion method as described in detail in [15], was used for synthesizing $\text{Li}_{0.5-0.5x}\text{Mg}_x\text{Fe}_{2.5-0.5x}\text{O}_4$ ($x = 0.0, 0.1, 0.4, 0.6, 0.8, 1.0$). For preparing the samples, AR grade citrate-nitrate precursors were dissolved in 10 ml de-ionized water in stoichiometric ratio. Honeys (as green fuel) were used to carry out green synthesis keeping metal salt to honey ratio as 1:1, and pH of the solution was not adjusted. Honey acts as chelating agent as well as fuel to facilitate the combustion process.. Resulting solution was heated at $\sim 110^\circ\text{C}$ to obtain fluffy powder called as 'dry gel', which was used for structural, magnetic studies.

Room temperature x-ray diffraction (XRD) measurements ($\theta - 2\theta$ configuration) were done by Bruker D8 diffractometer utilizing CuK_α radiation (wavelength: 0.15406 nm) equipped with fast counting detector (Bruker LynxEye detector). Hysteresis measurements were done by vibrating sample magnetometer (VSM) Lakeshore Model 7410 by applying maximum field - $H_{\text{max}} \approx \pm 1.9\text{ T}$.

Rietveld refinement of XRD patterns was done by MAUD (Material Analysis Using Diffraction) software [16] to compute experimental lattice parameter (a_{exp}). Specific surface area (S) was calculated using the expression: $S = [6 / (D_s \times \rho_{\text{XRD}})]$, where D_s – Scherrer's grain size and ρ_{XRD} - x-ray density. XRD peak intensities were used to obtain cation distribution of the studied samples, employing Bertaut method [17]. Obtained cation distribution was used to calculate theoretical lattice parameter (a_{th}), Néel magnetic moment (theoretical magnetization at 0 K $M_{\text{S}(0)}$) is calculated using formula: $n_N = M_B - M_A$ in Bohr magneton (μ_B) where M_A is magnetic moment of A-site and M_B is magnetic moment of B-site, oxygen positional parameter (u), inversion parameter (δ), ionic radius for A, B-site (r_A, r_B). Coercivity (H_c), saturation magnetization (M_s), magnetic losses were obtained from hysteresis measurements.

RESULTS AND DISCUSSION

The x-ray diffraction patterns of the synthesized samples (*by honey green synthesis, without any post-preparation thermal treatment*) confirm the formation of spinel phase shown in figure 1 (a) for Mg substituted Li ferrite. Via presence of important peaks corresponding to (220), (311), (222), (400), (422), (511), (440), planes confirms the formation of single phase face centered cubic structure. All parameters were calculated from most intense peak (311) of XRD pattern. Figure 1 (b) displays the Rietveld refinement of the X – ray diffraction pattern for $x = 0.0$, done by the program MAUD (Material Analysis Using Diffraction) [18].

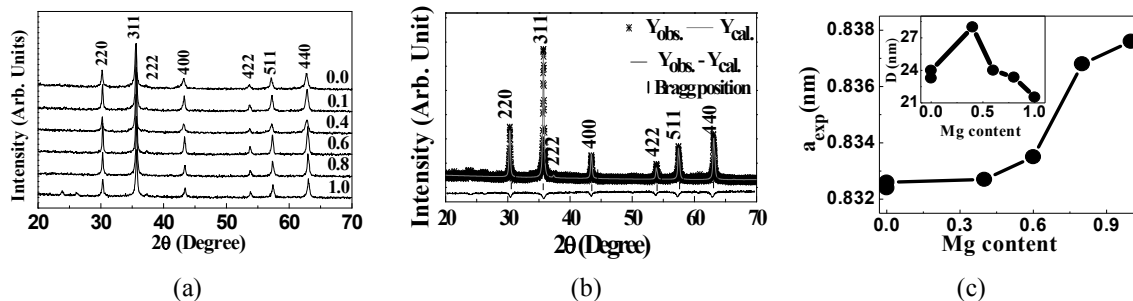


FIGURE 1. (a) XRD patterns of studied samples, (b) Rietveld refinement for $x=0.0$, (c) Variation of a_{exp} with Mg content Inset: Variation of D with Mg content.

Table 1. Compositional dependence of grain diameter (D), cell volume (V), x-ray density (ρ_{xrd}), specific surface area (S) and hopping length for A-site, B-site (L_A, L_B) for the studied samples.

x	D (nm)	V (nm ³)	ρ_{xrd} (kg/m ³)	S (m ² /g)	L _A (nm)	L _B (nm)
0.0	23.2	0.9330	2945.2	47.92	0.4232	0.3460
0.1	23.9	0.5774	4748.8	52.64	0.3605	0.2947
0.4	27.9	0.5774	4698.2	45.61	0.3605	0.2947
0.6	24.0	0.5791	4651.7	53.70	0.3609	0.2950
0.8	23.3	0.5860	4565.0	56.26	0.3623	0.2962
1.0	21.5	0.5878	4519.4	61.65	0.3627	0.2965

Figure 1 (c) shows the variation of experimental lattice parameter with Mg^{2+} content. Observed changes are attributed to the smaller ionic radius Fe^{3+} (0.064 nm), being replaced by Mg^{2+} (0.072 nm) ion which has higher ionic radius, causing expansion of unit cell.

Table 1 depicts, variation of grain diameter (D), cell volume (V), X-ray density (ρ_{XRD}), specific surface area (S), and hopping length for A-site (L_A), B-site (L_B) of studied samples. Perusal of table 1 shows that grain diameter obtained from Scherrer's formula varies between 21.5 to 23.2 nm. Observed cell volume, X-ray density (ρ_{XRD}) of Li-Mg ferrite increases with increasing Mg^{2+} content, attributed to the smaller ionic radius of Fe^{3+} (0.064 nm) is being replaced by an ion of greater ionic radius: Mg^{2+} (0.072 nm), that causes the expansion of tetrahedral, octahedral site. Specific surface area of the samples decreases for all values of x except for $x = 0.4$. High specific surface area of particles is useful for catalytic processes. There is an inverse relationship of particle size and density with surface area. In general, high surface areas suggests small particle size(s). Smaller is the particle size, larger is the surface area. The behavior of hopping length for tetrahedral and octahedral site with Mg content is similar with behavior of lattice parameter [19].

Table 2 depicts the distribution of cation: on A (tetrahedral site) are given in parentheses and the ions on B (octahedral sites) between the square bracket. The values of, theoretical lattice parameter (a_{th}), ionic radius of tetrahedral and octahedral site (r_A, r_B), inversion parameter (δ), oxygen positional parameter (u) with Mg^{2+} content were estimated by cation distribution. Obtained cation distribution shows that both Li^{1+} and Mg^{2+} ion prefer B site and a small fraction of Li^{1+} and Mg^{2+} ion goes on A site for sample $x = 0$ or $x > 0$ except in sample $x = 0.8$, in this sample large fraction Li^{1+} ion goes on tetrahedral site and small fraction goes on octahedral B site. The delta parameter (δ) is referred as inversion parameter. For a completely random distribution $\delta = 0.33$, for normal spinel $\delta = 1$ and for an inverse spinel $\delta = 0$. Delta parameter calculated from cation distribution initially shows completely inverse structure for $Li_{0.5-0.5x} Mg_x Fe_{2.5-0.5x} O_4$ ferrite but with the increasing Mg^{2+} content it shows mixed spinel structure for $\delta = 0.35$. The cation distribution obtained from the X-ray diffraction is in close conformity with the real distribution, as there is good agreement between theoretical (a_{th}) and experimental (a_{exp}) lattice parameter (shown in table 2).

The decrease of r_A is due the decrease in the concentration of larger Mg^{2+} ions (ionic radius = 0.072 nm) on A-site, which increases the concentration of smaller Fe^{3+} ions (ionic radius = 0.064 nm), but the same trend is not observed for the sample with $x = 0.8$ because of the fact that Mg^{2+} ions (0.072 nm) completely replaces the Li^{1+} ions and decreases the smaller Fe^{3+} ions (ionic radius = 0.064 nm) and, thus r_A increases.

Table 2. Cation distribution (for A, B site), inversion parameter (δ), experimental, theoretical lattice parameter (a_{exp}, a_{th}), ionic radii for A, B-sites, oxygen positional parameter (u) of $Li_{0.5-0.5x} Mg_x Fe_{2.5-0.5x} O_4$ ferrite as a function of Mg content.

x	Cation distributions	δ	a_{exp} (nm)	a_{th} (nm)	r_A (nm)	r_B (nm)	u
0.0	$(Li_{0.25}Fe_{0.75})^A [Li_{0.25}Fe_{1.75}]^B$	0.0	0.8324	0.8356	0.0515	0.0659	0.3814
0.1	$(Li_{0.25}Mg_{0.05}Fe_{0.7})^A [Li_{0.15}Mg_{0.05}Fe_{1.8}]^B$	0.05	0.8326	0.8351	0.0519	0.0655	0.3816
0.4	$(Li_{0.2}Mg_{0.2}Fe_{0.9})^A [Li_{0.1}Mg_{0.2}Fe_{1.7}]^B$	0.2	0.8327	0.8365	0.0516	0.0658	0.3821
0.6	$(Li_{0.05}Mg_{0.2}Fe_{0.75})^A [Li_{0.15}Mg_{0.2}Fe_{1.65}]^B$	0.2	0.8335	0.8356	0.0511	0.0662	0.3809
0.8	$(Li_{0.05}Mg_{0.3}Fe_{0.65})^A [Li_{0.05}Mg_{0.5}Fe_{1.45}]^B$	0.3	0.8368	0.8381	0.0519	0.0666	0.3810
1.0	$(Li_{0.0}Mg_{0.35}Fe_{0.65})^A [Li_{0.0}Mg_{0.65}Fe_{1.35}]^B$	0.35	0.8376	0.8387	0.0518	0.0669	0.3808

Table 3. Variation of coercivity (H_c), experimental saturation magnetization (M_s), magnetization at 0K ($M_{s(0K)}$), static magnetic losses, reduce remanence magnetization (M_r) and static losses as a function of Mg content.

X	H_c (Oe)	M_s (Am ² /kg)	$M_{s(th)}$ (Am ² /kg)	M_r (Am ² /kg)	M_r/M_s	Losses (J/Kg)
0.0	127.4	43.20	134.84	9.1	0.21	1.41
0.1	114.4	50.80	149.05	11.9	0.24	1.61
0.4	101.4	40.39	150.38	10.2	0.26	1.12
0.6	889.9	23.47	123.90	4.5	0.16	0.49
0.8	880.4	29.09	110.91	6.7	0.23	0.74
1.0	728.1	16.34	97.73	2.8	0.17	0.33

The ionic radius r_B are found to be increase, can be ascribed to the population of the substituted Mg^{2+} ions increases on *B-site* and Mg^{2+} (0.072 nm) ions are also occupied on *B-site*. The decrease of ionic radius on *B-site* (r_B) can be explain that for sample with $x = 0.8$, Li^{1+} ions are completely replace the Mg^{2+} ions. Oxygen position parameter (u) values varies between 0.3814 to 0.3808 which is higher than the ideal value of 0.375 for Li-Mg nanoferrites suggests that the movement of O^{2-} ions, so A-O distance increases, thus increasing distortion.

Table 3, shows coercivity (H_c), saturation magnetization (M_s) at 300 K, theoretical magnetization at 0 K ($M_{s(0)}$), remanence (M_r), squareness ratio (M_r/M_s), and static losses determined from the M–H curve of the studied Li-Mg ferrite system. It is worth noting that the Fe^{3+} ions occupy both A, B-sites in the spinel lattice, and they interact with each other through superexchange interaction: A - A, A - B and B - B with Li^{1+} ions occupy B-site in the spinel lattice whereas Mg^{2+} ions can occupy both the A and B-sites. Some of the doped Mg^{2+} ions displace the Fe^{3+} ions from A-site to B-site. The increase in M_s with increase in Mg^{2+} ion composition can be understood on the basis of redistribution of cations at A, B-sites. The resultant magnetization ' M_s ' (which is theoretical magnetization at 0K, expressed as $M_{s(0)}$) comes from the difference of B-site magnetization (M_B) and A-site magnetization (M_A), i.e., $M_s = M_B - M_A$. The octahedral (B-site) has larger magnetic moment than the tetrahedral (A-site), therefore the resultant magnetization increases, thereafter decreases with increasing Mg content, understood in terms of cation distribution

Figure 2(a), shows room temperature hysteresis loops for the studied samples confirms soft magnetic behavior of Li-Mg ferrite, shows compositional dependence of experimental M_s . Figure 4(b), displays that the experimental value of M_s at 300 K ranges between 16.34 – 50.80 Am²/kg and theoretical magnetization at 0 K: $M_{s(0)}$ varies between 97.73 – 150.38 Am²/kg, shown in figure 2 (b) for the studied samples decreases with increasing Mg^{2+} content, ascribable to reduction of Fe^{3+} (Magnetic moment: $5\mu_B$) population with concurrent increase of Mg^{2+} ions (Magnetic moment: $0\mu_B$) on B site. Similar trend of experimental M_s at 300 K (obtained from VSM measurements) and that of theoretical magnetization at 0 K: $M_{s(0)}$ (obtained from cationic distribution, computed from XRD measurements) shows that the magnetization behavior of the studied samples [18]. Observed similar trend of $M_{s(exp)}$, $M_{s(0)}$ shows that the magnetization behavior of the studied samples is governed by Néel model. Figure 2(b) inset gives M_s variation with δ , shows linear variation of M_s with δ , demonstrating the importance of δ in determining M_s . Figure 2 (c), shows linear variation of M_s , while variation of H_c is shown in inset, with increasing Mg^{2+} content.

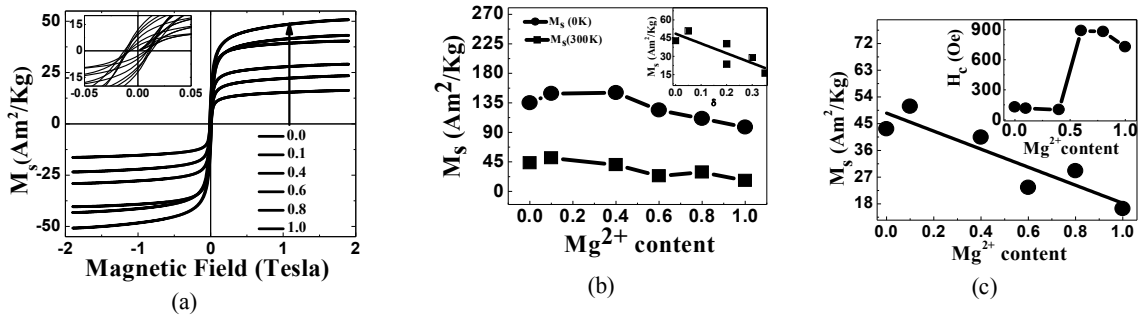


FIGURE 2. (a) Hysteresis loops, Inset: zoom part of hysteresis loops, (b) Experimental M_s at 300K and theoretical $M_{s(t)}$ at 0K. Inset : Linear variation of M_s with δ , (c) Linear variation of M_s with Mg content: Inset : Variation of H_c with Mg content

Initially value of H_c found to be decreases up to $x=0.4$, thereafter sharply increasing with highest value found to be 889.9 Oe originates from increasing anisotropy due to presence of Li^{1+} ions at octahedral [B] site [18,19]. The reason for decrease in coercivity up to $x=0.4$, with increasing Mg^{2+} in Li ferrite is the decrease in magneto-crystalline anisotropy by migration of Mg^{2+} ions to tetrahedral (A) site and by lowering the concentration of Fe^{3+} ions at octahedral sites in spinel lattice because Fe^{3+} ions are also the source of the magnetic anisotropy in ferrites.

SUMMARY

XRD validates the formation of single phase $\text{Li}_{0.5-0.5x}\text{Mg}_x\text{Fe}_{2.5-0.5x}\text{O}_4$ nano ferrite, via green synthesis protocol, without any post-preparation thermal treatment, whereas lattice parameter incorporation of Mg^{2+} ion in the spinel lattice. Observed alteration of cationic distribution proves transition from inverse to mixed spinel structure, and reflects in magnetic properties, modifying both M_s (*exp*), H_c , and also confirms that the magnetization behavior of the studied samples is governed by Néel model.

ACKNOWLEDGMENTS

We thank Dr. M. Gupta, UGC-DAE CSR, Indore for XRD data. SNK gratefully acknowledges one month invited professor stay at ENS Universite Paris-Saclay, Cachan (France), during Oct.-Nov. 2017.

REFERENCES

1. S. N. Kane and M. Satalkar, *J. Mater. Sci.* **52**, 3467–3477 (2017).
2. G. Busca, E. Finocchio, V. Lorenzelli, M. Trombetta, and S. A. Rossini, *J. Chem. Soc. Faraday Trans.*, **92**, 4687-4693 (1996).
3. K. An, and T. Hyeon, *Nanotoday*, **4**, 359-373 (2009).
4. Z. L. Wang, Y. Liu, Z. Zhang, Handbook of Nanophase and Nanostructured Materials. Vol. 3; Kluwer Academic/Plenum Publishers: New York, 2002.
5. L. Gastaldi, A. Lapicciarella,, *J. Solid State Chem.* **30**, 223–229 (1979).
6. D.V. Kurmude, R.S. Barkule, A.V. Raut, D.R. Shengule, K.M. Jadhav, *J. Supercond. Nov. Magn.* **27**, 547–553 (2013).
7. A. Najafi Birgani, M. Niyafar, A. Hasanpour, *J. Magn. Magn. Mater.* **374**, 179–181 (2015).
8. R. S. Yadav, I. Kuřitka, J. Vilcakova, J. Havlica, J. Masilko, L. Kalina, J. Tkacz, J. Švec, V. Enev and M. Hajdúchová, *Adv. Nat. Sci: Nanosci. Nanotechnol.* **8**, 045002–1–14 (2017).
9. D. Gingasu, L. Mindru, S. Preda, J. M. Calderonmoreno, D. C. Culita, L. Patron and L. Diamandescu, *Rev. Roum. Chim.*, **62**, 645–653 (2017).
10. M. S. Al-Qubaisi, A. Rasedee, M. H. Flaifel, S. H. J. Ahmad, S. Hussein-Al-Ali, M. Z. Hussein, E. E. M. Eid, Z. Zainal, M. Saeed, M. Ilowefah, S. Fakurazi, N. M. Isa and M. E. E. Zowalaty, *Int. J. Nanomedicine* **8**, 2497–2508 (2013).
11. M. K. Shobana, *Journal of Physics and Chemistry of Solids* **73**, 1040–1043 (2012).
12. P. Vijaya Bhasker Reddy, B.Ramesh , Ch.Gopal Reddy, *Physica B* **405**, 1852–1856 (2010).
13. S.C. Watawe, S. Keluskar, Gonbare, R. Tangsali, *Thin Solid Films* **505**, 168–172 (2006).
14. Akhter, M. A. Hakim, *Mater. Chem. Phys.* **120**, 399–403 (2010).
15. S. Panchal, S. Raghuvanshi, K. Gahlot, F. Mazaleyrat and S. N. Kane, *AIP Advances* **6**, 055930–6 (2016).
16. L. Lutterotti and P. Scardi, *J. Appl. Cryst.* **23**, 246-252 (1990).
17. E. F. Bertaut, *C. R. Acad. Sci.* **230**, 213 (1950).
18. R. Verma, S. N. Kane, S. Raghuvanshi, M. Satalkar, S. S. Modak and F. Mazaleyrat, *AIP Conf. Proc.* **1953**, 030135-1-030135-4 (2018).
19. S. Raghuvanshi, F. Mazaleyrat, and S. N. Kane, *AIP Advances* **8**, 047804–1-047804-11 (2018).